JOURNAL OF AIRCRAFT
Vol. 32, No. 1, January–February 1995

Application of Transonic Small Disturbance Theory to the Active Flexible Wing Model

Walter A. Silva* and Robert M. Bennett†
NASA Langley Research Center, Hampton, Virginia 23681

The CAP-TSD code, developed at the NASA Langley Research Center, is applied to the active flexible wing wind-tunnel model for prediction of transonic aeroelastic behavior. A semispan computational model is used for evaluation of symmetric motions, and a full-span model is used for evaluation of antisymmetric motions. Static aeroelastic solutions using the computational aeroelasticity program-transonic small disturbance, are computed. Dynamic (flutter) analyses are then performed as perturbations about the static aeroelastic deformations and presented as flutter boundaries in terms of Mach number and dynamic pressure. Flutter boundaries that take into account modal refinements, vorticity and entropy corrections, antisymmetric motions, and sensitivity to the modeling of the wingtip ballast stores are also presented and compared with experimental flutter results.

Introduction

AN understanding of the aeroelastic behavior of flight vehicles in the transonic Mach number regime is of great importance for flight safety. For example, it is well known that aircraft flying into or through the transonic regime may encounter a region of reduced flutter speed known as the transonic flutter dip. Valuable insight into the nature of this transonic flutter dip phenomenon is provided by Isogai[1] for a typical, two-dimensional streamwise section of an aft-swept wing, while a comparison of aerodynamic predictions with the experiments reported by Davis and Malcolm[2] reveals the limitations of linear theory when applied in the transonic regime. Linear aerodynamic predictions, although highly successful in the subsonic and supersonic regimes, normally cannot be used to predict transonic aeroelastic behavior accurately. Transonic flow equations capable of modeling flow nonlinearities (shocks, boundary layer, separation, and vorticity), and boundary conditions that induce nonlinear effects (airfoil thickness and shape, and large deflections), then must be solved. The surveys by Edwards and Malone[3] and Ballhaus and Bridgeman[4] review developments in the field of computational transonic aeroelasticity. Some of these developments include modeling of the Navier-Stokes equations[5] and the Euler equations[6] for flutter analysis. Application of these higher-order formulations to complete aircraft configurations have been limited due to the large computational resources required. Certain assumptions regarding the flow that results in reduced-order formulations such as the full potential equation[7] and the computationally efficient transonic small-disturbance (TSD) equation can be made. Research efforts involving the TSD formulation include the development of the XTRAN3S code,[8] the work by Yang et al.,[9] and many others.

The computational aeroelasticity program-transonic small disturbance (CAP-TSD) code was developed at the NASA Langley Research Center (LaRC). CAP-TSD is capable of analysis of configurations that have multiple lifting surfaces with control surfaces, bodies (nacelles, stores), vertical surfaces, and a fuselage, and solves the TSD equation using an efficient approximate factorization scheme.[10] References 11 and 12 verified the ability of the code to predict steady and unsteady pressures accurately for wings and configurations at subsonic, transonic, and supersonic Mach numbers. Flutter prediction using CAP-TSD for two thin, swept and tapered wings compared well with experimental flutter results.[13]

The goal of the present study was to update the transonic aeroelastic analysis of the active flexible wing (AFW) wind-tunnel model[14] that was reported in Ref. 15. The AFW model is a full-span, sting-mounted wind-tunnel model designed and built by the Rockwell International Corporation. A photograph of the AFW model can be seen in the accompanying editorial. The main goal of the AFW program was to design, implement, and validate digital control laws for flutter suppression[14] that could operate simultaneously with rolling maneuver control laws. Therefore, knowledge of possible regions of instability was desirable.

This article first presents the computational procedures contained in CAP-TSD. This includes a brief description of the TSD formulation and the coupled aerodynamic and structural equations of motion that are integrated in time. These equations were used for static and dynamic aeroelastic analyses of the AFW wind-tunnel model. An important conclusion of studies by Yates et al.[16] and Yates and Chu[17] was that the accuracy of the transonic flutter prediction is highly dependent on the accuracy of the static aeroelastic state of the wing. As a result, a procedure for computing static aeroelastic deformations[15] was applied to the AFW computational model. The dynamic behavior was computed as a perturbation about previously computed static aeroelastic solutions. The resultant dynamic time histories of the generalized displacements were then analyzed using a modal identification technique to estimate the stability parameters (damping and frequency) of the system at a given Mach number and dynamic pressure. Dynamic results are presented in the form of flutter boundaries, in terms of Mach number and flutter dynamic pressure. Flutter boundaries that account for corrected modeling[15] of the wingtip ballast store of the AFW wind-tunnel model, updated mode shapes and frequencies, vorticity and entropy corrections, and a subsonic antisymmetric flutter result, are presented and compared with experimental flutter results.

Computational Procedures

In this section, an overview of the computational procedures including a description of the CAP-TSD code, the aeroelastic equations of motion, the time-marching solution of these equations, and the modal identification of the resulting free decay transients are presented.

Received May 11, 1992; revision received March 7, 1994; accepted for publication March 21, 1994.

*Aerospace Engineer, Aeroelasticity Branch.
†Senior Aerospace Engineer, Aeroelasticity Branch. Associate Fellow AIAA.

TSD Equation

The CAP-TSD code is a finite difference program that solves the general-frequency modified TSD potential equation

$$M_\infty^2(\phi_t + 2\phi_x)_t = [(1 - M_\infty^2)\phi_x + F\phi_x^2 + G\phi_y^2]_x + (\phi_y + H\phi_x\phi_y)_y + (\phi_z)_z \quad (1)$$

where M_∞ is the freestream Mach number, ϕ is the disturbance velocity potential, and the subscripts of ϕ represent partial derivatives.

Several choices are available for the coefficients F, G, and H, depending upon the assumptions used in deriving the TSD equation. For current applications, the coefficients are defined as

$$F = -\tfrac{1}{2}(\gamma + 1)M_\infty^2$$
$$G = \tfrac{1}{2}(\gamma - 3)M_\infty^2 \quad (2)$$
$$H = -(\gamma - 1)M_\infty^2$$

where γ is the ratio of specific heats. The linear potential equation is recovered simply by setting F, G, and H equal to zero.

Equation (1) is solved within CAP-TSD by a time-accurate approximate factorization (AF) algorithm developed by Batina.[10] In Refs. 11–13, the AF algorithm was shown to be efficient for application to steady or unsteady transonic flow problems.

Several algorithm modifications have been made that improve the stability of the AF algorithm and the accuracy of the results.[18,19] Two of these improvements are vorticity and entropy corrections[19] for improved shock modeling. The effect of these corrections on the transonic flutter boundary of the AFW wind-tunnel model was investigated and is presented in a subsequent section of this article.

The CAP-TSD program can be used for analysis of configurations with combinations of lifting surfaces and bodies including canard, wing, tail, control surfaces, tip launchers, pylons, fuselage, stores, and nacelles. The configuration capability of the current version of CAP-TSD permits the calculation of pressures on the fuselage and bodies. In this version, however, modal perturbations of the fuselage and bodies were not included in the boundary conditions, and the integration of the pressures on the fuselage and on bodies (for computation of the generalized aerodynamic forces) was not included in the aeroelastic solution. However, the aerodynamic influence of the fuselage and the wingtip body of the AFW wind-tunnel model were included as interference effects upon the wing pressures.

Equations of Motion

The aeroelastic equations of motion are based on a right-hand orthogonal coordinate system with the x direction defined as positive downstream, the y direction positive out the right wing, and the z direction positive upward. The equations of motion may be written as

$$M\ddot{q} + C\dot{q} + Kq = Q \quad (3)$$

where q is a vector of generalized displacements, M is the generalized mass matrix, C is the generalized damping matrix, and K is the generalized stiffness matrix. Q is the vector of generalized forces where its elements are defined as

$$Q_i = \frac{\rho U^2}{2} c_r^2 \int_s \frac{\Delta p h_i}{\rho U^2/2} \frac{dS}{c_r^2}$$

Δp is the lifting pressure, ρ is the fluid density, c_r is the root chord, U is the freestream velocity, S is the area of the lifting surface(s), and h_i is the vibration mode shape. Equation (3) is rewritten as

$$\ddot{q} = -M^{-1}Kq - M^{-1}C\dot{q} + M^{-1}Q \quad (4)$$

to permit integration of the equation with respect to time.

Time-Marching Aeroelastic Solution

The aeroelastic solution procedure implemented within CAP-TSD for integrating Eq. (4) is similar to that described by Edwards et al.[20] Equation (4) is composed of normal mode equations that may be expressed in linear, first-order state-space form as

$$\dot{x}_i = Ax_i + Bu_i \quad (5)$$

where

$$x_i = (q_i \dot{q}_i)^T$$

$$A = \begin{bmatrix} 0 & 1 \\ -m_i^{-1}k_i & -m_i^{-1}c_i \end{bmatrix}$$

$$B = m_i^{-1} \frac{\rho U^2}{2} c_r^2 \begin{bmatrix} 0 \\ 1 \end{bmatrix}$$

$$u_i = \int_s \Delta C_p h_i \, dS/c_r^2$$

$$\Delta C_p = \frac{\Delta p}{\rho U^2/2}$$

In these definitions, m_i, c_i, and k_i are elements of the mass, damping, and stiffness matrices, respectively, corresponding to mode i. The analytical solution to Eq. (5) is found in Ref. 20, and a description of its numerical implementation in CAP-TSD is found in Ref. 13.

For aeroelastic analysis, two steps generally are required in performing the calculations. In the first step, the steady-state flowfield is calculated to account for wing thickness, camber, mean angle of attack, and static aeroelastic deformation, thus providing the starting flowfield for the dynamic aeroelastic analysis. Previously published CAP-TSD flutter studies, with the exception of Ref. 15, analyzed only symmetric wings at zero steady angle of attack,[13] thereby avoiding the problem of static aeroelastic deformations. For the AFW wind-tunnel model, the airfoil sections are not symmetric and the wing has twist. Thus, a procedure for computing static aeroelastic solutions had to be developed before an accurate dynamic analysis could be performed. The dynamic analysis then would be a perturbation about a converged static aeroelastic solution at each Mach number and dynamic pressure of interest.

The procedure developed[15] and applied in this study for computing static aeroelastic deformations is to allow the structure and aerodynamics to interact with no initial excitation (no initial deflection or velocity), and with a large value of viscous damping to prevent divergence of the solution. This method resulted in convergence of the generalized displacements. Static aeroelastic deformations should be independent of viscous damping and, therefore, different values of viscous damping (ζ = 0.375, 0.707, and 0.99) were evaluated. A typical result for this type of analysis is presented in Fig. 1, which shows a representative variation of a generalized displacement as a function of computational time steps for the three values of viscous damping. It is clear from Fig. 1 that the generalized displacements converged to a value that is independent of the value of viscous damping. Furthermore, the larger the value of viscous damping, the faster the convergence. Therefore, the highest value of viscous damping (ζ = 0.99) was used in order to accelerate the static aeroelastic

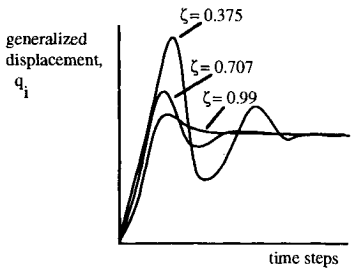

Fig. 1 Convergence of generalized displacements for different values of viscous damping.

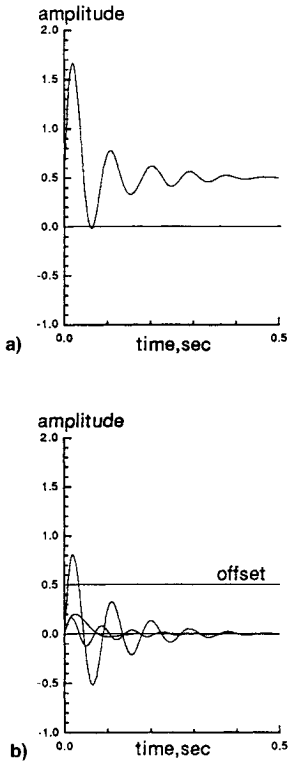

Fig. 2 Example of modal identification: a) aeroelastic transient and b) offset and identified modal components.

solution. For the applications presented herein, 2000–4000 time steps were used to converge the static aeroelastic solutions. All CAP-TSD solutions were computed on a Cray computer and averaged about 3.25 s/time step.

An interesting result of this procedure was that it allowed the computation of static aeroelastic deformations at dynamic pressures above the flutter dynamic pressure for the AFW wind-tunnel model. Once converged, static aeroelastic solutions were computed, the next step was to prescribe an initial disturbance to begin the dynamic structural integration. Modal velocities in the first three modes were used as initial perturbations. Approximately 7 cycles of the lowest frequency (first) mode were needed for accurate modal identification. For a constant, nondimensional time step of 0.01, this required 8000 time steps. In determining a flutter point, the freestream Mach number M_∞, and the associated freestream speed U, were held fixed. A value of the dynamic pressure, $q = \rho U^2/2$, then was used, and free decay transients were computed. These resulting transients of the generalized coordinates were analyzed for their content of damped or growing sine-waves, with the rates of decay or growth indicating whether the dynamic pressure was above or below the flutter value. This indicated whether to increase or decrease the value of dynamic pressure in subsequent analyses to determine a neutrally stable result.

Modal Identification

As previously mentioned, CAP-TSD generates free decay transients that must be analyzed for the modal stability characteristics. A typical transient for the AFW model, calculated using CAP-TSD, is shown in Fig. 2a. The first three modes used in the analysis were excited by specifying an initial condition for each modal velocity to produce a complex decay record. This record is analyzed using a least-squares curve-fit of the response data with complex exponential functions. The program utilized is a derivative of the one described in Ref. 21. The components of the transient of Fig. 2a are plotted in Fig. 2b to the same scale. The free decay properties of each mode for this condition are readily apparent, and the mean or offset value is the static aeroelastic deformation of the mode being analyzed. A sufficient range of dynamic pressure must be considered to determine all relevant flutter points.

Analysis and Results

CAP-TSD Computational Model

The AFW geometry data, including detailed airfoil shape information, was obtained from Rockwell International. From this geometry data, two computational models were generated. A half-span model, with a vertical plane of symmetry specified at the centerline, was used for symmetric analyses, and a full-span model was used for antisymmetric analyses. Both computational models consisted of a fuselage, a region aft of the main wing and next to the fuselage referred to as the coat-tail, the main wing(s) with four control surfaces per wing, and the wingtip ballast store(s). The four control surfaces per wing are the leading-edge inboard (LEI), leading-edge outboard (LEO), trailing-edge inboard (TEI), and trailing-edge outboard (TEO). Each control surface has a chord that is 25% of the local chord and a span that is 28% of the semispan. The airfoil definition includes the control surface actuator bumps on the outboard half of the wing. There are slight surface discontinuities on the wind-tunnel model where the wing box and control surfaces meet (at the quarter- and three-quarter-chord). These discontinuities are not included in the analytical model because of potential numerical difficulties. The effect of the actuator bumps and the control surface/wing box discontinuities on the measured and computed static pressure distributions will be presented in a subsequent section.

The grid dimensions for the half-span model are 134 × 51 × 62 in the x, y, and z directions, respectively, for a total of 423,708 grid points. The grid extends 10 root chords upstream, 10 root chords downstream, 2 semispan lengths in the y direction, and 10 root chords in the positive and negative z direction. The full-span grid is dimensioned 134 × 101 × 62 grid points in the x, y, and z directions (839,108 grid points). The wind-tunnel sting mount is modeled by extending the

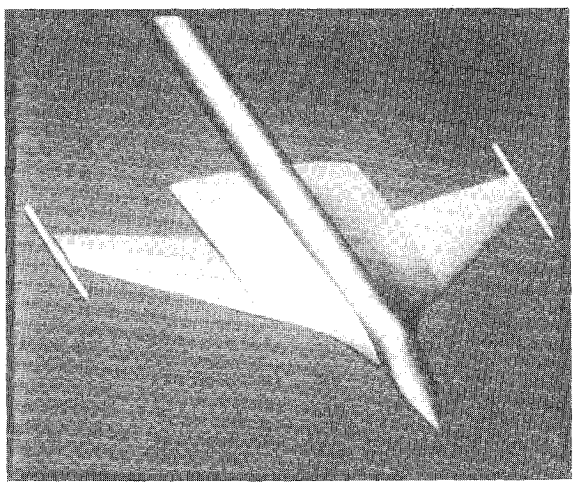

Fig. 3 CAP-TSD computational model of the AFW.

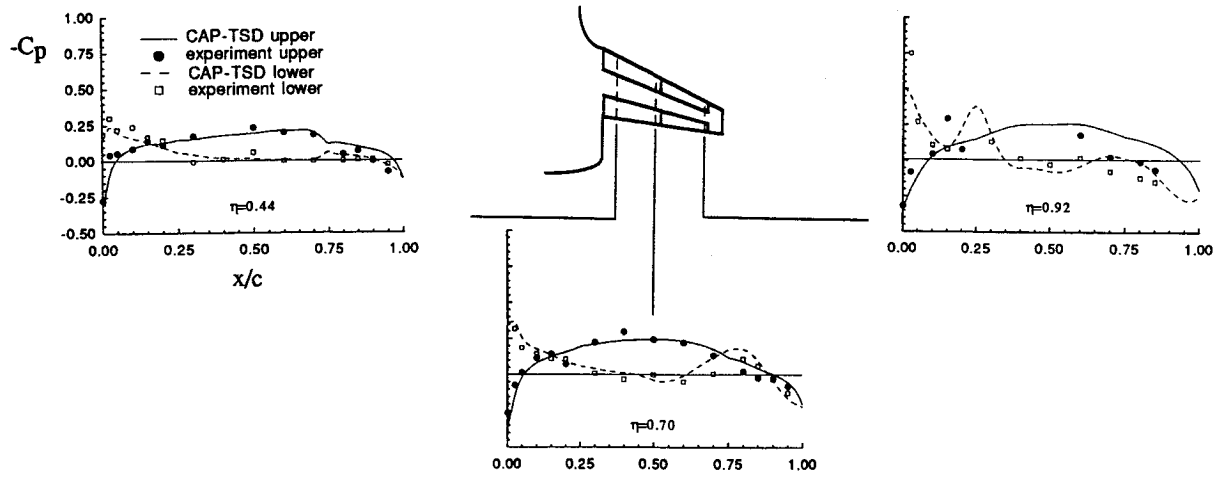

Fig. 4 Pressure distributions at $M_\infty = 0.9$ and $q = 150$ psf in a heavy gas.

computational fuselage aft to the downstream boundary of the grid. The grid density was increased in regions where large changes in the flow were expected, such as at the leading edge, trailing edge, wingtip, and control-surface sides and hinge lines.

A computer-generated image of the CAP-TSD model of the AFW wind-tunnel model is shown in Fig. 3. Although not shown in the figure, a protrusion on the underside of the fuselage that houses the model's pitch actuator is also included in the analytical model.

Analytical modes and frequencies were obtained from a finite-element model, that includes the mass of the tip ballast store, and separated into symmetric and antisymmetric modal data sets. The flutter analyses of Ref. 15 were performed using analytical mode shapes with measured frequencies (from a ground vibration test). Since the symmetric data were shown by linear analysis[14] to be the most flutter critical in the higher, subsonic Mach number regime, only symmetric motions were analyzed in Ref. 15 using the semispan model. Since then, an updated set of symmetric and antisymmetric mode shapes were generated based on experimental data. These updated mode shapes are defined for a denser set of structural points for improved accuracy in the interpolation procedure. The interpolation of mode shape displacements and slopes at the computational grid points was done via a surface spline.[22] Each structural section was splined separately and then recombined to form the necessary input to CAP-TSD. The separate structural sections are the wing box, coat-tail, and the four control surfaces. Slender bodies such as the fuselage and tip ballast store are not given any modal definition in CAP-TSD, as previously mentioned. Therefore, no modal data were needed for these components.

Static Results—Pressure Distributions

The accuracy of the static aeroelastic solution was investigated in Ref. 15 by comparing analytical results obtained using the original set of symmetric mode shapes with existing experimental data. Two sets of experimental data from previous AFW wind-tunnel tests in a heavy gas were used for this purpose. These data included 1) pressure coefficient distributions and 2) control-surface effectiveness parameters. In Ref. 15, by comparing calculated and experimental pressure distributions at a chosen Mach number and dynamic pressure, it was concluded that the static aeroelastic procedure provided reasonable estimates of the static aeroelastic deformation of the AFW wind-tunnel model using the original set of mode shapes. It also was concluded that comparisons of the calculated and experimental control surface effectiveness parameters were reasonable qualitatively, but were deficient quantitatively due to the lack of viscous effects in the CAP-TSD model. Therefore, in the present study, the accuracy of the static aeroelastic procedure is not reassessed, but instead only a comparison of calculated pressure distributions using the updated set of mode shapes and the experimental pressure distributions is presented. The AFW configuration for these previous tests did not include the tip ballast store used in the recent test, so that in order for the CAP-TSD calculations to compare with the earlier experiments, the tip ballast store was deleted from the computational model and replaced by a tip fairing.

Figure 4 presents pressure coefficient distributions vs fraction of chord for CAP-TSD with the updated set of mode shapes and experiment at $M_\infty = 0.9$ and a dynamic pressure of 150 psf at the three spanwise stations shown. As with the original set of mode shapes, the overall agreement between the most recent analysis and experiment is good, with some discrepancies occurring near the trailing edge and wingtip. The first two span stations compare reasonably well from the leading edge up to about 60% of the local chord. Sudden changes in the experimental data can be seen near the quarter-chord at the second span station, and near the three-quarter-chord for all three span stations. These disruptions in the flow may be caused by the previously-mentioned physical discontinuities where wing box and control surfaces meet. At the second and third span stations, the effect of the actuator bumps on the lower surface pressures is evident. Agreement between analysis and experiment deteriorates at the outboard span station, possibly due to separated and/or tip vortex flow around the wingtip region.

Comparisons of the static aeroelastic results using the updated structural model with those of the previous model of Ref. 15 show essentially the same behavior. There exists a slight difference between the two results at the first span station near the three-quarter-chord location where the updated structural model reveals the presence, or beginnings of, a shock that was not present with the original structural model. This appears to be a slight improvement in comparison with the test data. However, the exact cause of the sudden change in the experimental pressure distribution at this location is not clear, as it may be due to a shock or to the geometric discontinuity that exists at the quarter-chord and three-quarter-chord locations of the wing.

Dynamic Results—Symmetric Motions

Flutter dynamic pressures were computed at $M_\infty = 0.5, 0.9, 0.92, 0.93, 0.94$, and 0.95. The analyses that included the vorticity and entropy corrections were computed at $M_\infty = 0.5, 0.9, 0.92, 0.93$, and 0.95. The original flutter boundary computed prior to the 1989 wind-tunnel test includes a flutter dynamic pressure at $M_\infty = 0.975$. Although the results for all of these Mach numbers are included in the figures, results are discussed primarily for the $M_\infty = 0.5, 0.9, 0.93$, and 0.95 cases. All flutter analyses are for the AFW model in air at

1.5-deg angle of attack, and include a viscous damping of 0.015 (structural damping of 0.03) for all modes.

In Ref. 15, a rather severe transonic flutter dip was computed using the CAP-TSD code, and the bottom of this computational transonic flutter dip did not agree well with experiment. Figure 5, from Ref. 15, is a comparison of the CAP-TSD computed flutter boundary, the linear flutter boundary defined using the doublet lattice theory, and the experimental flutter results from the Fall of 1989 and the Spring of 1991 wind-tunnel tests. The doublet lattice model includes a lifting-surface modeling of the wingtip ballast stores.

Accounting for nonlinearities in the flow, by the application of the CAP-TSD code, is a clear improvement over the linear flutter predictions at transonic Mach numbers, since the CAP-TSD prediction indicated the presence of a severe transonic flutter dip. The no-flutter track, shown in the figure, is the path, in terms of Mach number and dynamic pressure, through which the wind tunnel proceeded for which no flutter was encountered. Therefore, this no-flutter track defines a lower bound for the bottom of the experimental transonic flutter dip, which disagrees with the bottom of the transonic flutter dip predicted using CAP-TSD. As a result, one of the goals of the present study was to investigate some of the possible causes of this discrepancy by modifying and improving specific elements of the analysis.

Corrected Tip Store Modeling

The first improvement to the analysis was the correction of an error in the modeling of the wingtip ballast store. The error consisted of a sign change in a portion of the slopes that geometrically define the tip store. The effect of this error was investigated, and the resultant flutter boundary for the corrected wingtip ballast store model is presented in Fig. 6 along with the original, uncorrected flutter boundary presented in Fig. 5. At $M_\infty = 0.5$, the effect of the corrected tip store model was to reduce the flutter dynamic pressure from 290 to 259 psf with a change in flutter frequency from 10.70 to 11.20 Hz. At this Mach number there was no change in the flutter mechanism from the mechanism reported in Ref. 15, which consisted of a classical coalescence of the first-bending mode and the first-torsion mode. The flutter dynamic pressure dropped only slightly at $M_\infty = 0.9$ from 190 to 182 psf, while at $M_\infty = 0.93$ the flutter dynamic pressure increased from 52 to 77 psf. The flutter dynamic pressure at $M_\infty = 0.95$ increased significantly from 81 to 133 psf. Again, the flutter mechanism at these three transonic Mach numbers was essentially the same as the mechanism reported in Ref. 15 for transonic Mach numbers, which consisted of a first-bending-dominated instability. The changes in flutter frequency at $M_\infty = 0.9$, 0.93, and 0.95 were, respectively, from 9.50 to 9.36 Hz, from 7.78 to 8.08 Hz, and from 8.07 to 8.83 Hz.

The corrected modeling of the wingtip ballast store therefore improved the flutter boundary by moving the flutter dynamic pressure in the direction of the experimental results at all Mach numbers. These results also indicate the sensitivity of the calculated flutter boundary to the modeling of tip aerodynamics at subsonic and transonic conditions. For all of the results that follow, the corrected modeling of the wingtip ballast store has been included.

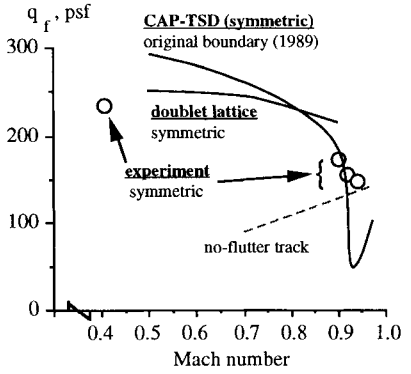

Fig. 5 Comparison of linear, nonlinear, and experimental flutter boundaries for original mode shapes.[15]

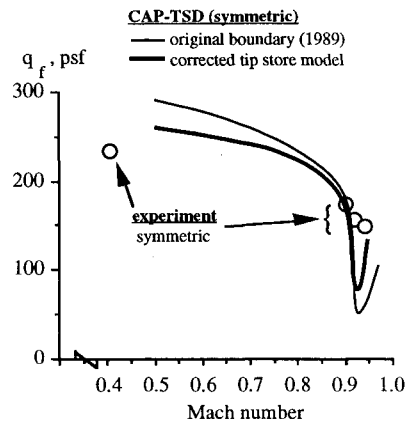

Fig. 6 The effect of the corrected tip store modeling on the symmetric flutter boundary using the original structural model.

Updated Mode Shapes and Frequencies

An updated and improved set of mode shapes and frequencies were obtained after the wind-tunnel test of 1989. The following improvements were made: 1) refinements to the structural model based on experimental data, and 2) a denser set of structural points for improved mode shape definition, in particular around the control surface regions and the wingtip region of the AFW wind-tunnel model.

The flutter boundary obtained using the updated structural model is shown in Fig. 7 and compared to that obtained using the original structural model (corrected tip store model from Fig. 6). There is an increase in flutter dynamic pressure at $M_\infty = 0.5$ with the new structural model. The increase in flutter dynamic pressure is from 259 to 281 psf with a decrease in flutter frequency from 11.20 to 10.86 Hz. At $M_\infty = 0.9$, the flutter dynamic pressure increases from 182 to 203 psf with a slight change in flutter frequency from 9.36 to 9.44 Hz. The flutter dynamic pressure at $M_\infty = 0.93$ increases significantly from 77 to 103 psf with an increase in frequency from 8.08 to 8.32 Hz. For $M_\infty = 0.95$ the flutter dynamic pressure also increases significantly from 133 to 183 psf with an increase in flutter frequency from 8.83 to 9.33 Hz.

The updated structural model brings the computational results into closer agreement with experimental results at transonic Mach numbers greater than $M_\infty = 0.9$. But at $M_\infty = 0.5$ and 0.9 the comparison with experiment is degraded. A possible reason for this deficiency in the CAP-TSD prediction is that the current version of the code treats bodies such as

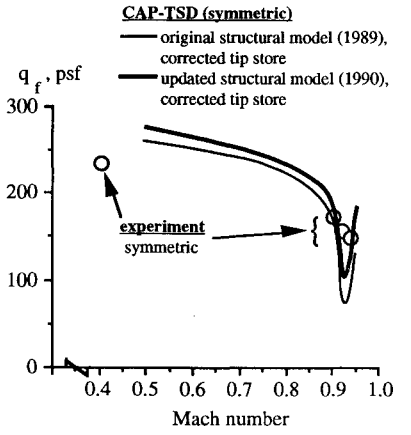

Fig. 7 Comparison of symmetric flutter boundaries for original (corrected) and updated structural models.

the wingtip ballast store and fuselage as aerodynamic influences with no modal definition. Although the effect of a modally-defined fuselage on the flutter boundary may be minimal, the effect of a modally-defined wingtip ballast store is probably significant, as can be seen by the sensitivity to changes in the modeling of the wingtip ballast store in Fig. 6. These effects should be investigated when a version of the CAP-TSD code becomes available that accounts for modal deformations of the fuselage and bodies, and thus, the contribution of these components to the generalized aerodynamic forces. Viscous effects, not accounted for in the current inviscid version of the code, also may have a significant effect on the subsonic and transonic flutter boundaries.

Vorticity and Entropy Corrections

The vorticity and entropy corrections defined in Ref. 19 and incorporated into current versions of the CAP-TSD code were applied with updated mode shapes and frequencies at M_∞ = 0.5, 0.9, 0.92, 0.93, and 0.95. These corrections typically reduce shock strength and shift the shock location forward. The resultant flutter boundary due to the implementation of these corrections is compared to the transonic portion of the flutter boundary for the updated structural model without vorticity and entropy corrections in Fig. 8. The effect of the corrections at M_∞ = 0.9 is minimal, lowering the flutter dynamic pressure from 203 to 200 psf, and reducing the flutter frequency from 9.44 to 9.40 Hz. The effects of the corrections are significant at M_∞ = 0.93, where the flutter dynamic pressure increased from 103 to 126 psf with an increase in flutter frequency from 8.32 to 8.53 Hz. An interesting effect is noticed at M_∞ = 0.95, in that the flutter dynamic pressure is reduced from 183 to 130 psf and the flutter frequency drops from 9.33 to 8.60 Hz. The effect of the vorticity and entropy corrections is therefore significant, in that it improves the correlation with experiment at the transonic Mach numbers evaluated. The inclusion of vorticity and entropy also tends to widen the rather steep and narrow transonic flutter dip previously computed (Figs. 5–7).

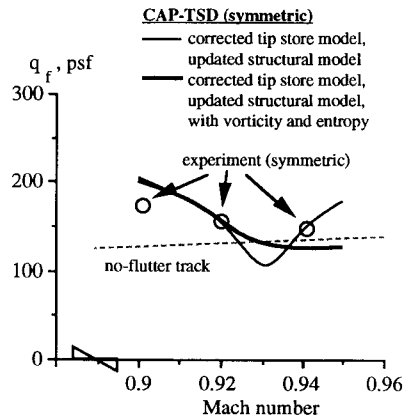

Fig. 8 Experimental and computational symmetric flutter boundaries with and without vorticity and entropy corrections.

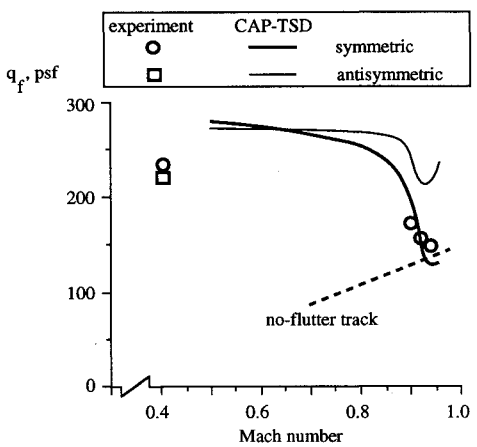

Fig. 9 Comparison of calculated symmetric and antisymmetric flutter boundaries with experimental results.

In general, for symmetric motions, the effects of improved and updated analyses resulted in excellent agreement with experiment at transonic conditions while resulting in some degradation of the comparisons at M_∞ = 0.5 and 0.9. It is possible that accounting for the modal definition of the wingtip ballast store will provide some insight into this discrepancy. It is also interesting to note that the computational result at M_∞ = 0.92 is insensitive to the computational modifications and improvements described above, and compares extremely well with experiment. At this Mach number, the calculated flutter dynamic pressure, for the vorticity and entropy case, e.g., is 151 psf, which differs only slightly from the experimental flutter value of 156 psf.

Dynamic Results—Antisymmetric Motions

In order to generate antisymmetric aeroelastic responses, a full-span model of the AFW wind-tunnel model was generated. A progressive verification of the full-span model and of the capability of the CAP-TSD code for handling full-span aeroelastic analyses was deemed necessary before any antisymmetric flutter analyses were performed. This progressive verification proceeded as follows. First, a full-span, rigid, and steady solution was compared to a semispan, rigid, and steady solution at the same Mach number. Lift and pitching moment coefficients for both cases were identical, thereby verifying the aerodynamic modeling of the full-span model and the accurate implementation of the symmetric boundary condition for the semispan model. Second, static aeroelastic solutions were computed for both models using symmetric modes at a chosen Mach number and dynamic pressure. Again, the resultant lift and pitching moment coefficients, including static aeroelastic deformation of both models, were in exact agreement, verifying the modal definition of the full-span model. Finally, a full-span, symmetric dynamic analysis was compared to a semi-span, symmetric dynamic analysis resulting in identical transients, verifying the full-span model for dynamic analyses.

An important aspect of the antisymmetric flutter analyses was the necessary addition of symmetric mode shapes to the aeroelastic modeling along with the antisymmetric mode shapes. The reason for this is that since dynamic analyses are computed about converged static aeroelastic solutions and since static aeroelastic solutions are symmetric for a vehicle defined symmetrically about its centerline, antisymmetric dynamic analyses require the inclusion of symmetric modes as well. The computational model therefore consisted of 10 symmetric modes needed for static aeroelastic solutions, and 10 antisymmetric modes needed for the dynamic aeroelastic solutions. These additional modes did not increase the computer time significantly as the finite difference solution of Eq. (1) dominated the CPU time.

Figure 9 is a comparison of the nonlinear CAP-TSD symmetric flutter boundary for the updated set of mode shapes with vorticity and entropy corrections (Fig. 8), the nonlinear CAP-TSD antisymmetric flutter boundary and the symmetric and antisymmetric experimental flutter points. Although the CAP-TSD-predicted antisymmetric flutter dynamic pressure of 272 psf at M_∞ = 0.5 is significantly higher than the experimental value of 219 psf at M_∞ = 0.4, the CAP-TSD analyses indicate that the antisymmetric instability is lower in flutter dynamic pressure than the symmetric instability at M_∞ = 0.5, but higher in flutter dynamic pressure than the symmetric instability at M_∞ = 0.9. This is consistent with the experimental results. The discrepancy between the CAP-TSD results at M_∞ = 0.5 and the subsonic experimental flutter results may be due to the lack of modal definition of the wingtip ballast store and, thus, its contribution to the unsteady gen-

eralized forces in the CAP-TSD computations. The effect of a modally-defined wingtip ballast store on the subsonic and transonic CAP-TSD flutter boundaries still needs to be investigated. Furthermore, viscous effects have not been addressed by the analyses presented thus far, and need to be investigated as well.

Concluding Remarks

In this study, the calculated symmetric aeroelastic behavior of the AFW wind-tunnel model using the CAP-TSD code was updated. In addition, the full-span, antisymmetric aeroelastic capability of the code was evaluated, and symmetric and antisymmetric results were compared with experimental flutter data.

The updated dynamic analyses consisted of modifications and improvements to key elements of the aeroelastic modeling. These modifications and improvements included a corrected aerodynamic modeling of the wingtip ballast store, an updated structural model, and the addition of vorticity and entropy corrections.

A static aeroelastic procedure previously developed was applied to an updated structural model. Results compared favorably with experimental data from a previous AFW wind-tunnel test. Static aeroelastic solutions therefore provided reasonable estimates of the static aeroelastic deformation of the wing. Dynamic analyses then were performed as perturbations about converged static aeroelastic solutions.

The corrected modeling of the wingtip ballast store resulted in improved correlation with subsonic and transonic symmetric experimental flutter points. The significant sensitivity of the aeroelastic analyses to changes in the modeling of the wingtip ballast store was revealed. The updated structural model improved the correlation with experiment at transonic Mach numbers, but degraded the correlation with experiment at the subsonic condition. The addition of vorticity and entropy corrections provided further improvements in the correlation with experiment at transonic Mach numbers. This is an indication of the importance of including vorticity and entropy effects in the computations.

A full-span computational model of the AFW wind-tunnel model was generated and used for computing an antisymmetric flutter boundary. Deficiencies in the correlation with experiment at $M_\infty = 0.5$ may be due to the lack of modal definition in the aerodynamics of the wingtip ballast store, which might have a significant effect on the generalized aerodynamic forces of the vehicle. Viscous (boundary-layer) effects, not accounted for in the CAP-TSD code, may also play an important role in both the subsonic and transonic regimes.

Acknowledgments

The authors would like to acknowledge B. Perry III and S. R. Cole of the NASA Langley Aeroservoelasticity Branch and the Configuration Aeroelasticity Branch, respectively, for providing experimental flutter data.

References

[1]Isogai, K., "On the Transonic-Dip Mechanism of Flutter of a Sweptback Wing," *AIAA Journal*, Vol. 17, No. 7, 1979, pp. 793–795.

[2]Davis, S. S., and Malcolm, G. N., "Experiments in Unsteady Transonic Flow," AIAA Paper 79-0769, April 1979.

[3]Edwards, J. W., and Malone, J. B., "Current Status of Computational Methods for Transonic Unsteady Aerodynamics and Aeroelastic Applications," NASA TM 104191, Dec. 1991.

[4]Ballhaus, W. F., and Bridgeman, J. O., "Numerical Solution Techniques for Unsteady Transonic Problems," AGARD Rept. 679, Paper 16, March 1980.

[5]Wu, J. C., Kaza, K. R. V., and Sankar, N. L., "A Technique for the Prediction of Airfoil Flutter Characteristics in Separated Flows," AIAA Paper 87-0910, April 1987.

[6]Bendiksen, O. O., and Kousen, K., "Transonic Flutter Analysis Using the Euler Equations," AIAA Paper 87-0911, April 1987.

[7]Shankar, V., and Ide, H., "Unsteady Full Potential Computations Including Aeroelastic Effects," *Proceedings of the 5th International Conference on Numerical Methods in Laminar and Turbulent Flow*, Vol. 5, Pt. 2, Pineridge Press, Swansea, Wales, UK, 1987, pp. 1944–1954.

[8]Borland, C. J., and Rizzetta, D. P., "Nonlinear Transonic Flutter Analysis," *AIAA Journal*, Vol. 20, No. 11, 1982, pp. 1606–1615.

[9]Yang, T. Y., Guruswamy, P., and Striz, A. G., "Application of Transonic Codes to Flutter Analysis of Conventional and Supercritical Airfoils," *Proceedings of AIAA Dynamics Specialist Conference* (Atlanta, GA), AIAA, New York, 1981, pp. 332–342 (AIAA Paper 81-0603).

[10]Batina, J. T., "Efficient Algorithm for Solution of the Unsteady Transonic Small-Disturbance Equation," *Journal of Aircraft*, Vol. 25, No. 7, 1988, pp. 598–605.

[11]Batina, J. T., Seidel, D. A., Bland, S. R., and Bennett, R. M., "Unsteady Transonic Flow Calculations for Realistic Aircraft Configurations," *Journal of Aircraft*, Vol. 26, No. 1, 1989, pp. 21–28.

[12]Bennett, R. M., Bland, S. R., Batina, J. T., Gibbons, M. D., and Mabey, D. G., "Calculation of Steady and Unsteady Pressures on Wings at Supersonic Speeds with a Transonic Small-Disturbance Code," *Journal of Aircraft*, Vol. 28, No. 3, 1991, pp. 175–180.

[13]Bennett, R. M., Batina, J. T., and Cunningham, H. J., "Wing Flutter Calculations with the CAP-TSD Unsteady Transonic Small-Disturbance Program," *Journal of Aircraft*, Vol. 26, No. 9, 1989, pp. 876–882.

[14]Perry, B., III, Cole, S. R., and Miller, G. D., "A Summary of the Active Flexible Wing Program," AIAA Paper 92-2080, April 1992.

[15]Silva, W. A., and Bennett, R. M., "Predicting the Aeroelastic Behavior of a Wind-Tunnel Model Using Transonic Small-Disturbance Theory," ICAS Paper No. 90-1.1.1, Sept. 1990.

[16]Yates, E. C., Jr., Wynne, E. C., and Farmer, M. G., "Measured and Calculated Effects of Angle of Attack on the Transonic Flutter of a Supercritical Wing," NASA TM 83276, Aug. 1982.

[17]Yates, E. C., Jr., and Chu, L., "Static Aeroelastic Effects on the Flutter of a Supercritical Wing," NASA TM 89132, March 1987.

[18]Batina, J. T., "Unsteady Transonic Algorithm Improvements for Realistic Aircraft Applications," *Journal of Aircraft*, Vol. 26, No. 2, 1989, pp. 131–139.

[19]Batina, J. T., "Unsteady Transonic Small-Disturbance Theory Including Entropy and Vorticity Effects," *Journal of Aircraft*, Vol. 26, No. 6, 1989, pp. 531–538.

[20]Edwards, J. W., Bennett, R. M., Whitlow, W., Jr., and Seidel, D. A., "Time-Marching Transonic Flutter Solutions Including Angle-of-Attack Effects," *Journal of Aircraft*, Vol. 20, No. 11, 1983, pp. 899–906.

[21]Bennett, R. M., and Desmarais, R. N., "Curve Fitting of Aeroelastic Transient Response Data with Exponential Functions," *Flutter Testing Techniques*, NASA SP-415, May 1975, pp. 43–58.

[22]Harder, R. L., and Desmarais, R. N., "Interpolation Using Surface Splines," *Journal of Aircraft*, Vol. 9, No. 2, 1972, pp. 189–191.